ELSEVIER

Catalysis Today 50 (1999) 479–500

CATALYSIS TODAY

Towards more realistic computational modeling of homogenous catalysis by density functional theory: combined QM/MM and ab initio molecular dynamics

T.K. Woo, P.M. Margl, L. Deng, L. Cavallo[1], T. Ziegler*

Department of Chemistry, University of Calgary, 2500 University Drive, NW, Calgary, Alta., Canada T2N 1N4

Abstract

The combined quantum mechanics/molecular mechanics (QM/MM) and the ab initio molecular dynamics methods (AIMD) are fast emerging as viable computational molecular modeling tools. Both methods allow for the incorporation of effects that are often ignored in high level calculations, but may be critical to the real chemistry of the simulated system. In the combined QM/MM method part of the system, say the active site, is treated quantum mechanically whereas the remainder of the system is treated with a faster molecular mechanics force field. This allows high level calculations to be performed where the effects of the environment are incorporated in a computationally tractable manner. With the ab initio molecular dynamics methods, the system is simulated at a finite temperature with no empirical force field. Rather, the forces at each time step are determined with a full electronic structure calculation at the density functional level. Thus, simulations of chemical reactions can be performed where finite temperature effects are realistically represented. In this paper a brief introduction to both methods is given. The methods are further demonstrated with specific applications to modeling homogenous catalytic processes at the molecular level. These applications are our latest efforts to build more realistic computational models of catalytic systems at the density functional level.

Keywords: QM/MM; AIMD; Ab initio molecular dynamics

1. Introduction

Homogenous catalytic systems have often been used to model more complicated heterogeneous systems. However, even seemingly simple homogenous systems pose many challenges for computational quantum chemists. Often times a first-principle's quantum mechanical calculation involves a stripped down model that only vaguely resembles the true system. If large ligand systems are involved they are most often neglected in high level calculations with the hope that they do not substantially influence the nature of the reaction mechanisms. Unfortunately, the surrounding ligand system, solvent or matrix can often play a critical mechanistic role. One reasonable approach to constructing a more sophisticated computational model which approximates these effects is the combined quantum mechanics and molecular mechanics (QM/MM) method [1–3], which has recently received significant attention in addressing these issues [4]. In this hybrid method part of the molecule, such as the active site, is treated quantum

*Corresponding author.

[1]Present address: Dipartimento di Chimica, Università "Federico II" di Napoli, Via Mezzocannone 4, I-80134 Naples, Italy.

0920-5861/99/$ – see front matter
PII: S0920-5861(98)00483-0

mechanically while the remainder of the system is treated with a molecular mechanics force field. This allows extremely large systems that are out of the reach of pure QM calculations to be studied in an efficient and detailed manner. In addition to neglecting solvent or ligand effects, many conventional electronic structure studies involve the exploration of the potential energy surface at the zero temperature limit. Therefore, finite temperature (non-zero) effects are neglected. Ab initio molecular dynamics methodologies allow for the exploration of potential energy surfaces of chemical reactions at finite temperatures. In this paper we attempt to review our experiences with the application of the QM/MM and AIMD methodologies to transition metal homogenous catalysis. Additionally, we intend to provide an elementary introduction to these methodologies since they are somewhat novel.

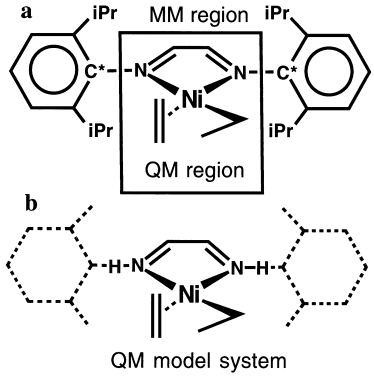

Fig. 1. (a) An example of a QM/MM partitioning in a Ni-diimine olefin polymerization catalyst. This structure represents the "real" system; (b) The corresponding model QM system for which the electronic structure calculation is performed. The hydrogen atoms cap the electronic system and are termed "dummy" atoms. The dummy atoms correspond to "link" atoms in the real system that are labeled C^* in (a).

2. The combined QM/MM method

The combined QM/MM involves determining the part of the potential energy surface of a system by an electronic structure calculation and the rest of the molecular potential by a molecular mechanics force field calculation. Successful synthesis of the two methods has the promise of allowing bond breaking and forming processes of extended systems to be simulated in computationally tractable times. The approach is guided by the idea that large systems can be partitioned into a region which necessitates a quantum mechanical description (the active site) while the remainder of the systems acts only as a perturbation to the QM region and therefore can be approximated adequately by a molecular mechanics description [5]. If the partition is made between separate molecules, then the combined QM/MM method is rather straightforward since the two regions interact only through non-bonded terms. Such QM/MM methods, therefore, concentrate on the appropriate representation of the intermolecular interactions and have been successfully applied to study solvation effects, most notably by Gao and coworkers [4,6,7]. However, if the partition occurs within the same molecule as illustrated in Fig. 1 the coupling of the two methods is substantially more difficult and dubious. The difficulty lies in the fact that at least one covalent bond will involve an atom from the QM region and one from the MM region. A number of combined QM/MM approaches have been developed to tackle this problem, with significant contributions from Warshel and Levitt [8], Singh and Kollman [1], Field et al. [2], Théry et al. [9] and Maseras and Morokuma [3].

By way of example, we will describe the QM/MM method with particular focus on how to deal with the QM/MM covalent bond. Fig. 1(a) depicts a Ni-diimine olefin polymerization catalyst, which is partitioned into a quantum mechanics (QM) region and a molecular mechanics (MM) region. There are two C^*–N bonds labeled that cross the QM/MM boundary with the N atom residing in the QM region and the C^* atom of the bond contained in the MM region. The immediate problem that arises is how to truncate the electronic system of the QM region across the C^*–N bonds. If the MM subsystems were simply removed, the unfilled valences left to the QM region would pose significant problems in a standard electronic structure calculation ultimately resulting in an unphysical picture. The simplest approach and the approach we have adopted to overcoming this truncation problem is to cap the electronic system with "dummy" hydrogen atoms as shown in Fig. 1(b). The capped system in Fig. 1(b) forms what is termed the model QM system for which a standard electronic structure calculation is per-

formed. It is assumed that the capped QM systems with the molecular mechanics region acting as a perturbation represents an adequate model of the electronic structure of the active site within the real system.

In the QM/MM method, the energy and gradients of the ''whole'' system are a hybrid or ''melting pot'' of the energy and gradients derived from the QM and MM calculations. The hybrid gradients and energies are then used to perform geometry optimization, transition state searches, or to perform molecular dynamics on the system as a whole. More formally, the total energy and gradients of the whole system can be expressed as

$$E_{\text{total}} = E_{\text{QM}} + E_{\text{MM}}, \tag{1}$$

$$\frac{\partial E_{\text{total}}}{\partial x_i} = \frac{\partial E_{\text{QM}}}{\partial x_i} + \frac{\partial E_{\text{MM}}}{\partial x_i}, \tag{2}$$

where the subscript QM refers to the energy and gradients derived from the electronic structure calculation, whereas the MM subscript refers to the energy and gradient terms derived from a force field calculation. In Eq. (2), the total gradients (or forces) on the MM atoms are only derived from the molecular mechanics calculation whereas the gradients on the QM atoms are the sum of the gradients resulting from the electronic structure calculation and the molecular mechanics calculation. When the QM/MM boundary crosses a covalent bond, Eqs. (1) and (2) present some problems. The first problem is which molecular mechanics potentials should be used to described the potential within the QM region and how should the QM and MM gradients be combined. For example, the Ni–N bond in the QM region of Fig. 1 can be described by both the electronic structure calculation on the model system and by an MM Ni–N bond stretching potential. Of course, if both contributions were included this would result in a redundant and likely unphysical description of the bond. This leaves the issue of which molecular mechanics potential energy contributions to include in the E_{MM} and which to discard. MM potentials which strictly involve MM atoms and therefore are in no way treated by the model QM system must be included. For example, this would include the C–C bond stretches in the aryl ring of Fig. 1(a) and the non-bonded interactions between the two aryl rings. On the other hand, molecular mechanics potentials which only involve QM atoms, such as the Ni–N stretch are assumed to be adequately treated by the QM calculation. Therefore, it would be redundant to superimpose a molecular mechanics Ni–N stretching potential on the existing QM potential. When an MM potential term contains both MM and QM atoms, such as the H–N–Ni bend potential the issue of whether to include the potential becomes ambiguous and this is where the different implementations of the QM/MM method vary. We will describe the two approaches that we have adopted to date.

In the scheme originally proposed by Singh and Kollman [1] all MM potential terms which contain at least one MM atom are included. Thus, the C^*–N bond stretch is handled by an MM C–N stretching potential. Here the C^*–N bond is not coupled to the N–H_{dummy} bond in the QM model system. In one sense this is appropriate since the C^*–N stretching frequency does not resemble that of the N–H_{dummy} bond. On the other hand, if the system is such that the C^*–N bond vector is severely distorted from that of the N–H_{dummy} bond vector as illustrated in Fig. 2, this distortion has no implications to the electronic structure of the model system. ''Resistance'' to the distortion is approximated by various MM potential terms such as an out of plane bending potential.

In the prescription of Maseras and Morokuma, a different approach is taken. In this approach the so-called ''link'' atom, C^* in this case, is always placed along the bond vector of the N–H_{dummy} bond and correspondingly all MM forces acting on the link atom are transferred (in a mathematically rigorous fashion) to the dummy atom of the QM system. ''Resistance'' to the distortion is not accounted for by MM poten-

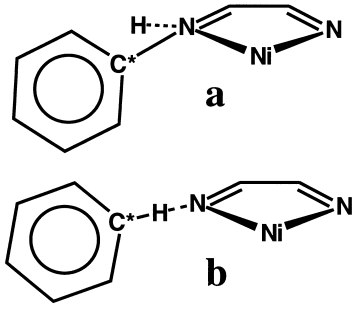

Fig. 2. Coupling of the atoms in covalent bonds which cross the QM/MM boundary.

tials, but is passed onto quantum mechanical system. Therefore, all MM potentials modeled by the QM system are not included.[2] For example, the C*–N–Ni MM bending potential is assumed to be adequately approximated by the "H–N–Ni QM" potential and is therefore not included. One advantage of this approach is that distortions such as that described in Fig. 2 are transferred to the electronic structure of the QM system. However, with this approach the link bonds become unphysical because they are coupled to dummy atom bonds.

Up to this point, we have described the case where the molecular mechanics region does not perturb the electronic structure of the QM region directly (simple mechanical embedding). Indirectly, the forces acting on the QM atoms resulting from the MM potentials can distort the geometry, however, the actual wavefunction or electron density is not perturbed directly by the MM subsystem. Polarization of the QM system by the MM region can be approximated by electrostatic interactions using, for example, point charges on the MM atoms which enter the Hamiltonian of the QM system. In the case of the DFT Kohn–Sham Hamiltonian, the point charges would enter as an external potential

$$\hat{H} = -\frac{1}{2}\nabla^2 + \sum_{I}^{N_{\mathrm{QM}}} \frac{Z_I^{\mathrm{QM}}}{|\mathbf{R}_I - \mathbf{r}|} + \int \frac{\rho'(\mathbf{r}')}{|\mathbf{r} - \mathbf{r}'|}\,\mathrm{d}\mathbf{r}' + V_{xc}(\mathbf{r}) + \sum_{\gamma}^{N_{\mathrm{MM}}} \frac{q_\gamma^{\mathrm{MM}}}{|\mathbf{R}_\gamma - \mathbf{r}|}. \quad (3)$$

The last term represents the external potential due to the point charges assigned to the QM atoms. (There would of course also be QM nuclear–MM point charge interaction potential). A host of problems arise with the electrostatic coupling of the QM and MM subsystems. The difficulties originate in assigning suitable point charges that are realistic and conserve the total charge of the whole system. Many potential improvements in the QM/MM methodology lie in refining the electrostatic coupling between the two subsystems. A good discussion of this can be found in [5,10].

[2]There is one exception. The non-bonded interactions between link atom and the QM atoms are included.

2.1. Limitations of the QM/MM method

There are of course many limitations to the combined QM/MM approach both those inherent in the QM and MM methods themselves and those which are a consequence of the union of the two. (The limitations of the QM and MM methods themselves are well known and therefore will not be elaborated upon here.) The overriding problem with the QM/MM method is that the interaction between the QM and MM regions is only approximate. Unfortunately, there is no "clean" way of treating these interactions and no rigorous formalism for improving it. Therefore, results should be validated and examined with care.

Since the electronic system of the MM atoms is not treated explicitly, electronic effects such as charge transfer, bond breakage/formation, conjugation or induction across the QM/MM interface cannot be modeled rigorously. Thus, judicious partitioning of the QM and MM regions is necessary for the method to be applied successfully. Specifically, the interface must be far enough removed from the reaction center so that there is no significant charge transfer across the boundary during the simulation, but at the same time, the QM region cannot be inhibitively large. Another limitation that the combined QM/MM method has is that absolute energies can only be compared for systems with the same number of QM/MM junctions with the same groups involved at the junctions. One reason for this is that the number and nature of the QM/MM junctions greatly affects the absolute electronic energies of the QM region.

It should also be realized that when a standard molecular mechanics force field such as MM2 or CHARMM is utilized, the parameters are not optimized to be used in a combined QM/MM treatment. Furthermore, molecular mechanics force fields are not fit to the same Born–Oppenheimer potential surface of a standard QM calculation. Instead, these force fields are generally fit to room temperature data resulting in an incompatibility. This is probably not a serious problem, but it is noteworthy. The hybrid QM/MM potential can be used just as any other potential energy surface is used to locate minimum energy geometries, to locate transition states, to construct reaction profiles or to perform dynamics simulations. The one limitation may be in using the hybrid potential to derive

frequencies because of the problems associated with the potentials at the interface bonds.

Combined QM/MM is ideal for simulating large aperiodic systems with an isolated reaction center such as metalloproteins, heterogeneous catalysts, surface reactions and solvent simulations. We have recently applied the QM/MM methodology to study a homogenous catalytic system with an extended ligand system that is too large to study at the full QM level.

3. Application of the QM/MM method to homogenous catalysis

Most applications of the QM/MM methodology (where the boundary cuts covalent bonds) have been concentrated in the area of protein modeling [11–15]. To date applications to transition metal-based catalysis have been limited. Morokuma et al. have demonstrated the methodology to the organometallic reaction of $Pt(PR_3)_2+H_2$ [16]. We have recently applied the QM/MM methodology to examine the role of the bulky substituents in the Brookhart Ni-diimine olefin polymerization catalyst [17].

3.1. *Brookhart's olefin polymerization catalyst: a QM/MM study*

Ni(II) diimine-based single site homogenous catalysts of the type (ArN=C(R)–C(R)=NAr)Ni–R'^{+} have emerged as promising alternatives to both traditional Ziegler–Natta and metallocene catalysts for olefin polymerization [18–20]. Brookhart and coworkers have shown that these catalysts are able to efficiently convert ethylene into high molecular weight polymers with a controlled level of polymer branching. In this polymerization system the bulky aryl groups play a crucial role, since without the bulky substituents the catalyst acts only as dimerization catalysts due to the favorability of the β-elimination chain termination process. From the structure of the catalyst, it is evident that the bulky aryl substituents partially block the axial coordination sites of the Ni center. It is likely that this steric feature which impedes the termination to the insertion process thereby promoting the intrinsically poor polymerization catalyst into a commercially viable one.

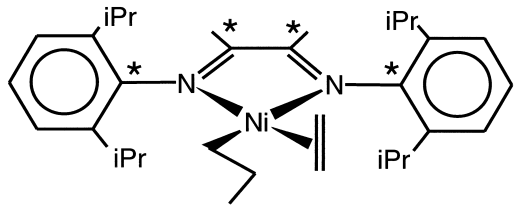

Fig. 3. Model for the active complex in the Brookhart Ni-diimine olefin polymerization system. The growing chain is modeled with a propyl group while the monomer is taken as an ethene. Atoms highlighted with an asterisk represent link atoms that are replaced by dummy hydrogen atoms in the model QM system.

With the propose of examining, in detail, the role of the bulky substituents in the Brookhart polymerization catalyst we have performed both pure QM calculations of the system without the bulky ligands and combined QM/MM calculations on the ''real'' system. In the QM/MM model, the bulky R=Me and Ar=2,6-$C_6H_3(i\text{-}Pr)_2$ groups are treated by the AMBER95 molecular mechanics potential whereas the Ni-diimine core including the growing chain and monomer are treated by a density functional potential. Fig. 3 shows the full catalyst system examined where the carbon atoms with asterisks represent the link atoms at the QM/MM boundary which are replaced by dummy hydrogen atoms in the QM model system.

Using the prescription of Maseras and Morokuma [3] we have combined the AMBER95 [21] molecular mechanics force field with the Amsterdam density functional (ADF) [22,23] program system. The QM system was calculated at the non-local density functional level with Becke's [24] 1988 exchange and Perdew's [25,26] 1986 correlation functionals. Full computational details are provided elsewhere [17].

Three processes are believed to dominate the polymerization chemistry of the catalyst system, namely, chain propagation, chain termination and chain branching, as shown in Fig. 4. The propagation commences from an olefin π-complex which has been determined experimentally to be the catalytic resting state. Insertion of the olefin into the M–C_α bond forms a metal alkyl cation. Uptake of the monomer returns the system to the resting state. Chain termination occurs via monomer assisted β-elimination, either in a fully concerted fashion as illustrated in Fig. 4(b), or in a multistep associative mechanism as implicated by Johnson et al. [19]. The unique short chain branch-

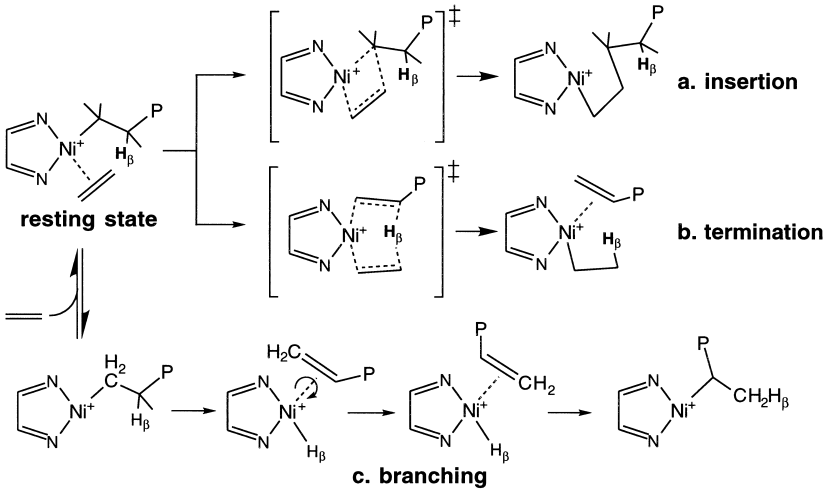

Fig. 4. Proposed reaction mechanisms of (a) insertion, (b) chain termination and (c) chain branching mechanisms for the Brookhart Ni-diimine olefin polymerization catalyst.

ing is proposed to occur via an alkyl chain isomerization process as sketched in Fig. 4(c). In this proposed process, β-hydride elimination first yields a putative hydride olefin π-complex. Rotation of the π-coordinated monomer followed by rotation yields a secondary carbon unit and therefore a branching point. It is important to note that the branching process commences from the Ni-alkyl cation and not the resting state complex. Since monomer pressure effects the branching rate, the equilibrium between the free Ni-alkyl and the resting state is believed to strongly influence the branching rate. Experimentally the relative magnitudes of the free energy barriers are ordered such that propagation<branching<termination.

Table 1 compares the reaction barriers, $\Delta H^{\ddagger}$, for the propagation, branching and termination processes for both the pure QM model with no ligands modeled and the QM/MM model. Without the bulky ligands, the termination barrier is approximately 30 kJ/mol less than the insertion (propagation) barrier, suggesting that the system would be a poor polymerization catalyst. This is in agreement with the experiment, where the Ni and Pd diimine systems without the bulky ligands are used as dimerization and oligermization catalysts [29]. When the bulky ligands are included, the termination and insertion barriers reverse their orders with a dramatic increase in the termination barrier. The termination transition state which is shown in Fig. 5(a) has both axial coordination sites of the Ni occupied. As proposed by Brookhart and coworkers [19,20] the bulky iso-propyl groups on the aryl rings act to block the axial coordi-

Table 1
Comparison of calculated and experimental barriers

	Reaction barriers (kJ/mol)		
	Insertion	Branching	Termination
Absolute			
Pure QM[a] ($\Delta H^{\ddagger}$)	70.3	53.6	40.6
QM/MM ($\Delta H^{\ddagger}$)	55.3	64.0	77.9
Experimental[b] ($\Delta G^{\ddagger}$)	42–46	–	–
Relative to insertion			
QM/MM ($\Delta\Delta H^{\ddagger}$)	0.0	8.8	22.6
Experimental[c] ($\Delta\Delta G^{\ddagger}$)	0.0	5.4[d]	23.4[e]

[a] From Ref. [27].
[b] From Ref. [28].
[c] From Ref. [20]. Polymerization of 1.6×10^{-6} mol of $(ArN{=}C(R)C(R){=}NAr)Ni(CH_3)(OEt_2)]^+[B(3,5\text{-}C_6H_3(CF_3)_2)_4]^-$ where Ar=2,6-C_6H_3(*i*-Pr)$_2$ and R=Me in 100 ml of toluene at 0°C for 15 min.
[d] NMR studies provide a ratio of 48 isomerization events per 500 insertions, assuming that all branches are methyl branches (methyl branches are experimentally observed to predominate). Applying Boltzmann statistics to this ratio at 273.15 K yields a $\Delta\Delta G$ of 5.4 kJ/mol.
[e] The weight-average molecular weight, M_w, of 8.1×10^5 g/mol provides an estimate for the ratio of termination events to insertion events of 1:28 900. Using Boltzmann statistics to this ratio gives a $\Delta\Delta G$ of 23.4 kJ/mol.

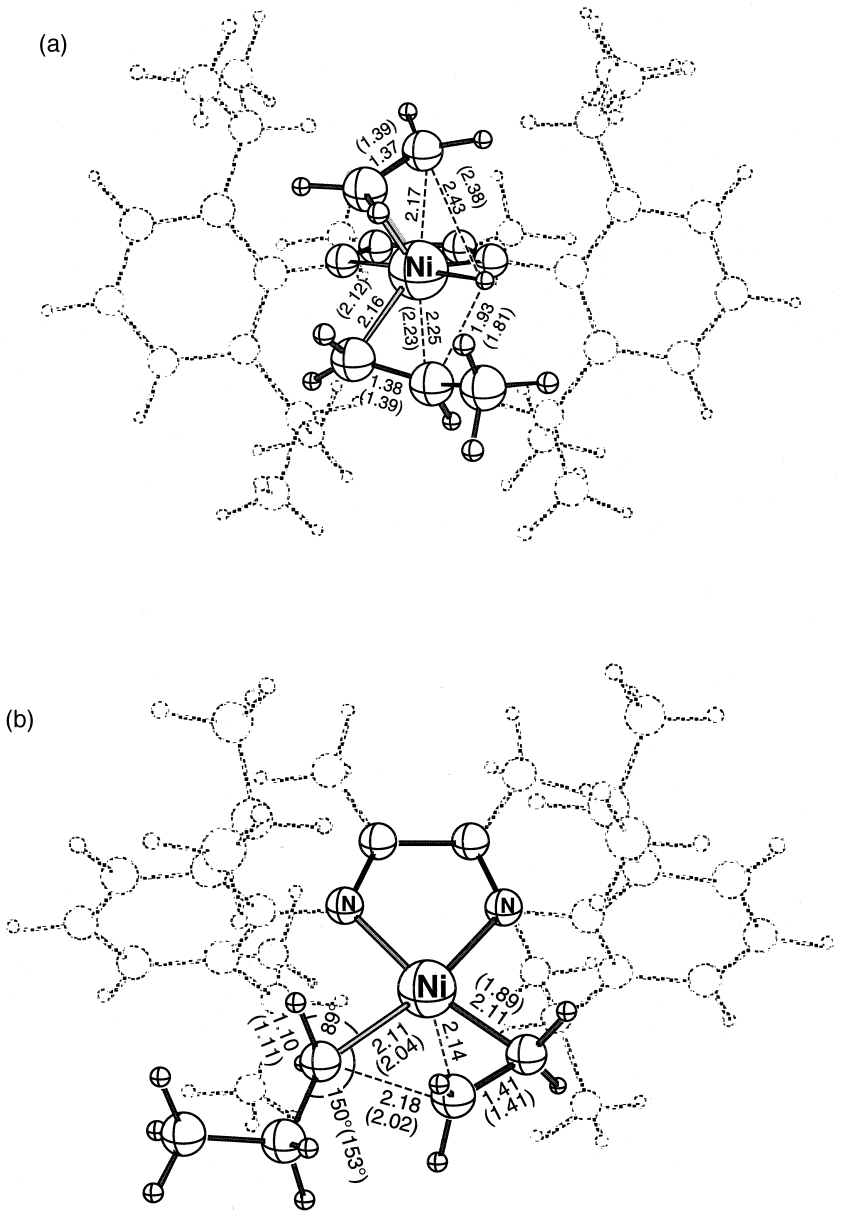

Fig. 5. Optimized QM/MM (a) chain termination transition state via β-hydrogen transfer to the monomer and (b) insertion transition state. MM atoms are ghosted for clarity, while the dummy hydrogen atoms are omitted. Parenthetic values refer to the same geometric parameter found in the corresponding pure QM geometry. The pure QM model does not contain the bulky ligands. Distances are in Ångstroms and angles in degrees.

nation sites thereby dramatically increasing the termination barrier. In the insertion transition state which is sketched in Fig. 5(b) the alkyl and olefin moieties lie in the coordination plane of the Ni center, removed from the bulky iso-propyl groups. In this case there is little steric hindrance to the insertion process. In fact the addition of the bulky aryl ligands actually reduces the insertion barrier. This stabilization of insertion transition state with bulky ligands in the QM/MM model compared to that without the bulky ligands

results from two effects. First, the resting state structure is destabilized by the bulky ligands, thereby lowering the insertion barrier by increasing the energy of the precursor. Additionally, there is the relaxation of the orientation of the aryl rings relative to the Ni-diimine ring in the insertion transition state. Physically, there is a preference for the aryl rings and the diimine ring to be more parallel to maximize the π-bonding between the rings. When both axial coordination sites are occupied as in the resting state and the termination transition state, the aryl rings are forced to be perpendicular to the diimine ring. In the insertion transition state where the axial sites are empty, the aryl rings can rotate away from the perpendicular orientations as to enhance the π-bonding interaction between the rings, thereby stabilizing the insertion transition state. This concept helps rationalize the observed [19] increase in activity when the π-system of the diimine ring is extended. We conclude that the catalyst activity can be increased by enhancing the π-bonding interaction between the diimine rings and the aryl rings.

The chain branching mechanism originally proposed by Brookhart and coworkers [19] involves discrete olefin hydride intermediate as sketched in Fig. 4(c). Our calculations implicate a concerted pathway since no stable olefin hydride complex could be located. (The optimized QM/MM chain branching transition state is not displayed.) With the hybrid model, the chain isomerization barrier is calculated to be 64 kJ/mol, which is only slightly increased from 53.6 kJ/mol in the pure QM model.

Table 1, reveals that the reaction barriers calculated from our combined QM/MM model are in good agreement with the experimentally determined free energy barriers, both in relative and absolute terms. This contrasts the results of the pure QM study where the bulky ligands were not modeled and even the order of the barrier heights is not reproduced. We note that there is an excellent agreement between the calculated and experimental chain termination barrier relative to the insertion barrier. Specifically, the QM/MM relative barrier is $\Delta\Delta H^{\ddagger}$=22.6 kJ/mol whereas the value determined experimentally is $\Delta\Delta G^{\ddagger}$=23.4 kJ/mol. Our model therefore provides an accurate estimate of the polymer molecule weight, M_w. It is more difficult to directly compare the calculated barriers for chain branching with that of the experiment because in our model we do not account for concentration effects. Fig. 4(c) shows that the branching commences from the metal–alkyl complex and there is an equilibrium between with the olefin coordinated π-complex. Experimentally, the chain branching increases with decreased monomer pressure, suggesting that the equilibrium between the π-complex and the metal–alkyl is crucial To address this issue we are currently simulating the olefin capture process with the combined QM/MM ab initio molecular dynamics method [30,31].

The QM/MM methodology has been successfully applied to examine the chemistry of the Brookhart Ni(II) diimine catalyst for which at least semi-quantitative results have been obtained. Moreover, we have demonstrated that the combined QM/MM method can be effectively applied to transition metal-based catalytic processes in a detailed yet efficient manner.

4. Ab initio molecular dynamics simulations

4.1. What is molecular dynamics?

Conventional electronic structure calculations can be classified as static simulations. In these calculations the nuclear positions are optimized to locate local minima and transition states on the potential surface at the zero temperature limit. This involves, for each nuclear geometry, converging the electronic structure in order to determine the energy and forces on the nuclei. This information is then used to move the nuclei to a more optimal geometry. In classical molecular dynamics the nuclei are allowed to move on the potential surface according to Newton's classical laws of motion (Eq. (4)) as to simulate nuclear motion at finite (non-zero) temperatures

$$m_i\mathbf{a}_i = \mathbf{F}_i(t) = -\frac{\partial E_{\mathrm{TOT}}}{\partial \mathbf{x}_i}, \quad i = 1, 2, \ldots, N_{\mathrm{nuc}}. \qquad (4)$$

The nuclear motion generated in a molecular dynamics simulation can be utilized for a variety of purposes. Stationary points can be optimized by simply applying friction to the nuclear motion, thereby causing the system to settle into a local minimum. The motion can also be used to sample configuration space as to construct a partition function from which properties can be derived rigorously from statistical

mechanics. There are also global minimization schemes which utilize molecular dynamics, such as simulated annealing. In this section our intent is to briefly introduce the basic concepts involved with ab initio molecular dynamics and particularly those issues specific to our simulations of homogenous catalytic systems.

The motion of the nuclei in a MD simulation is determined by integrating Newton's equations of motion (Eq. (4)). In other words, given the velocities and positions at a time t, one determines the same quantities with reasonable accuracy at a later time $t+\Delta t$ using the calculated forces on the nuclei. With each new geometry that is generated, the forces on the nuclei have to be recalculated. In order to simulate molecular vibrations, the time step Δt must be at least a third smaller than the period of the fastest vibration. Thus in order to simulate C–H bond stretching which has a period of 0.01 ps, the Δt must be roughly 0.003 ps. Even a relatively short 10 ps simulation requires over 3300 time steps and therefore 3300 gradient calculations. (To put this in perspective, even the fastest enzyme catalyzed reactions have turnover periods of greater than 1000 ps.) For this reason, most MD simulations are performed with a molecular mechanics force field. Their computational simplicity allows for extremely large simulations to be performed including protein folding processes. However, the empirical nature of molecular mechanics force fields has its limitations. For example, transition metal complexes which are of interest in our research are problematic because there is currently no force field general enough to handle all of the complicated bonding schemes available to these complexes. Moreover, chemical reactions cannot be simulated accurately (if at all) with a molecular mechanics force field. To overcome these problems ab initio or QM potentials can be used in conventional classical molecular dynamics. In other words, with the ab initio molecular dynamics (AIMD) method the forces are *not* determined from a molecular mechanics force field, but rather they are derived from a full electronic structure calculation at each time step. Although this is computationally demanding, it allows for bond breaking and forming processes to be simulated and it allows for molecular dynamics to be performed on systems where a molecular mechanics force field is not readily applicable.

4.2. Car–Parrinello ab initio molecular dynamics

Conventional AIMD involves moving the nuclei with the forces calculated from an electronic structure calculation. The electronic structure is normally described by a set of orthonormal molecular orbitals, φ_i, which are expanded in terms of a basis set, χ_k such that $\varphi_i = \sum_k c_{ik}\chi_k$. The optimal coefficients are solved variationally with the constraint that the molecular orbitals remain orthogonal. Generally this is done in a self-consistent manner by the diagonalization of the Hamiltonian matrix or equivalent. An alternative method for determining the optimal coefficients draws analogy to nuclear dynamics which is used to optimize nuclear geometries. By assigning fictitious masses to the coefficients, fictitious dynamics can be performed on the coefficients which then move through electronic configuration space with forces given by the negative gradient of the electronic energy. The equivalent equations of motion are

$$\mu\ddot{c}_{i,k} = -\frac{\partial E^{\mathrm{el}}}{\partial c_{i,k}} = -\sum_j \lambda_{i,j} c_{i,k} \langle \Psi_i | \Psi_k \rangle, \tag{5}$$

where μ is a fictitious mass, $\ddot{c}_{i,k}$ the coefficient acceleration, and the last term corresponds to the constraint force imposed to maintain orthogonality. The coefficients move through electronic configuration space with a fictitious kinetic energy and by applying friction the coefficients can be steadily brought to settle into an optimal configuration.

In 1985 Car and Parrinello [32] developed a scheme by which to perform the nuclear dynamics and the electronic coefficient dynamics in parallel as to improve the efficiency of the AIMD method. In this way the electronic MD and nuclear MD equations are coupled

$$\mu\ddot{c}_{i,k} = -\frac{\partial E}{\partial c_{i,k}} - \sum_j \lambda_{i,j} c_{i,k}, \qquad m_I \ddot{x}_I = -\nabla E(x_I, c_{i,k}).$$

Formally, the nuclear and electronic degrees of freedom are cast into a single, combined Lagrangian

$$\mathscr{L} = \sum \mu_i \langle \dot{\Psi}_i | \dot{\Psi}_i \rangle + \tfrac{1}{2} \sum M_I \dot{R}_I^2 - E_{\mathrm{DFT}}(|\Psi\rangle, R) + \sum_{i,j} \Lambda_{ij} \big(\langle \Psi_i | \Psi_j \rangle - \delta_{ij} \big), \tag{6}$$

where the first two terms represent the kinetic energy of the wavefunction and nuclei, respectively, the third

term is the potential energy and the last term accounts for the orthogonality constraint of the orbitals. The combined Car–Parrinello Lagrangian ensures that the propagated electronic configuration corresponds to the propagated nuclear positions. Although, the generated electronic configuration does not always correspond to the proper Born–Oppenheimer wavefunction, over time it generates an electronic structure that oscillates around it giving rise to stable molecular dynamics. The coupled Car–Parrinello dynamics, therefore, results in a speed up over conventional AIMD since the electronic wavefunction does not have to be converged at every time step, instead it only has to be propagated. The primary disadvantage of the Car–Parrinello MD scheme is that the electronic configuration oscillates about the Born–Oppenheimer wavefunction at a high frequency. Therefore, in order to generate stable molecular dynamics a very small time step must be used, usually an order of magnitude smaller than in conventional ab initio molecular dynamics.

Although other ''first-principles'' methods can be used, the Car–Parrinello coupled dynamics approach has mostly been implemented within the density functional framework with plane wave basis sets (as opposed to atom centered basis sets). Therefore, Car–Parrinello ab initio molecular dynamics generally refers only to this type of implementation. Applications of the Car–Parrinello AIMD method are concentrated in the area of condensed phase molecular physics.

The use of plane waves has its advantages in that the computational effort for the required integrations becomes minute on a per function basis. On the other hand, an enormous number of plane waves is required even when pseudopotentials are utilized to approximate the core. The number of plane waves required to accurately treat transition metals and first row elements becomes inhibitively large. This is clearly a problem in our research on homogenous catalysis since such systems almost always contain transition metals and the substrates are often made up of first row elements. Plane wave basis sets also introduce another problem when studying homogenous catalysts since periodic images are created automatically and therefore the simulation actually describes a periodic crystal. If non-periodic systems are simulated, then the cell size of the periodic systems must be sufficiently large that the wavefunctions of the images no longer overlap. This requires a vacuum region of approximately 5 Å between images. This is an issue because the computational effort increases with the cell size. If charged systems or systems with large dipole moments are simulated, the long range electrostatic interactions between periodic images will lead to artificial effects. Again, this is problematic in our research since many transition metal catalysts are charged species.

4.3. *Projector augmented wave (PAW) Car–Parrinello AIMD*

The projector augmented wave (PAW) Car–Parrinello AIMD program developed by Peter Blöchl overcomes the aforementioned problems such that AIMD simulations of transition metal complexes has become practical. PAW utilizes a full all-electron wavefunction with the frozen core approximation which allows both accurate and efficient treatment of all elements including first row and transition metal elements. In the PAW method, the plane waves are augmented with atomic-based functions near the nuclei such that the rapidly oscillating nodal structure of the valence orbitals near the nuclei are properly represented. One can think of it as smoothly stitching in an atomic-like function into the plane waves such that the plane waves describe regions where the orbitals are smooth, allowing for rapid convergence of the plane waves. The plane wave expressions of PAW and those of the pseudopotential method are similar enough that the numerical techniques for the most computationally demanding operations are related and equally efficient. Therefore, PAW combines the computational advantages of using plane waves with the accuracy of all-electron schemes. The details of the implementation are described elsewhere [33–35]. To deal with charged systems, PAW has a charge isolation scheme to eliminate the spurious electrostatic interactions between periodic images. The charge isolation scheme involves fitting atomic point charges such that the electrostatic potential outside the molecule is reproduced (ESP fit). The ESP charges are then used to determine the electrostatic interaction between periodic images via Ewald sums. The spurious interactions between images is then subtracted. These features of the PAW AIMD package make it ideal

to study transition metal catalysts at the ab initio molecular dynamics level.

4.4. Reaction free energy barriers with AIMD

Reaction free energy barriers are routinely calculated from conventional static electronic structure calculations. Here, the excess free energy of the reactants and transition state can be determined by constructing a partition function from a frequency calculation and using a harmonic (normal mode) approximation. In most cases where the interactions are strong, the approximation is good. However, for processes where weak intermolecular forces dominate, the harmonic or quasi-harmonic approximation breaks down [36]. Alternatively, ab initio molecular dynamics simulations can be utilized to determine reaction free energy barriers. An MD simulation samples the available configuration space of the system as to produce a Boltzmann ensemble from which a partition function can be constructed and used to determine the free energy. However, finite MD simulations can only sample a restricted part of the total configuration space, namely the low energy region. Since estimates of the absolute free energy of a system requires a global sampling of the configuration space, only relative free energies can be calculated.

A number of special methodologies have been developed to calculate relative free energies. Since we are interested in reaction free energy barriers, the method we use in our research is derived from the technique of thermodynamic integration and is often termed the potential of mean force method [37,38]. Assuming we are sampling a canonical NVT ensemble the free energy difference, ΔA, between an initial state with λ=0 and a final state with λ=1, is given by the following equation:

$$\Delta A_{(0\rightarrow 1)} = \int_0^1 \frac{\partial A(\lambda)}{\partial \lambda}\, \mathrm{d}\lambda. \tag{7}$$

Here the continuous parameter λ is such that the potential $E(\lambda)$ passes smoothly from initial to final states as λ is varied from 0 to 1. Since the free energy function can be expanded in terms of the partition function

$$A(\lambda) = -kT \ln\left[\int \cdots \int \exp - (E(X^N, \lambda)/kT)\, \mathrm{d}X^N\right] \tag{8}$$

the relative free energy ΔA can be rewritten as

$$\Delta A_{(0\rightarrow 1)} = \int_0^1 \left(\int \cdots \int \frac{\partial E(X^N, \lambda)}{\partial \lambda}\, \mathrm{d}X^N \Big|_\lambda \right) \mathrm{d}\lambda, \tag{9}$$

or

$$\Delta A_{(0\rightarrow 1)} = \int_0^1 \left\langle \frac{\partial E(X^N, \lambda)}{\partial \lambda} \right\rangle_\lambda \mathrm{d}\lambda, \tag{10}$$

where the subscript λ represents an ensemble average at fixed λ. Since the free energy is a state function λ can represent any pathway, even non-physical pathways. However, if we choose λ to be a reaction coordinate as to represent a physical reaction path, this provides us with a means of determining an upper bound for a reaction free energy barrier by means of thermodynamic integration. The choice in reaction coordinate is important since a poorly chosen reaction coordinate will result in an unfavorable reaction path and potentially a significant over estimate of the barrier. The more the reaction coordinate resembles the intrinsic reaction coordinate (IRC) the potentially better the estimate. The reaction coordinate can be sampled with discrete values of λ on the interval from 0 to 1 or carried out in a continuous manner in what is termed a ''slow growth'' simulation [39,60] by

$$\Delta A = \sum_{i=1}^{N_{\mathrm{steps}}} \langle f_\lambda \rangle_i \Delta\lambda_i, \tag{11}$$

where i indexes the step number and f_λ is the force on the constraint. Here the free energy difference becomes the integrated force on the reaction coordinate and can be thought of as the work necessary to change the system from the initial to final state. The discrete sampling resembles a linear transit calculation such that a series of simulations is set up corresponding to successive values of the reaction coordinate from the initial to final state. For each sample point, the dynamics must be run long enough to achieve an adequate ensemble average force on the fixed reaction coordinate. In a slow growth simulation [39] the reaction coordinate is continuously varied throughout the dynamics from the initial to the final state. Thus, in each time step the reaction coordinate is

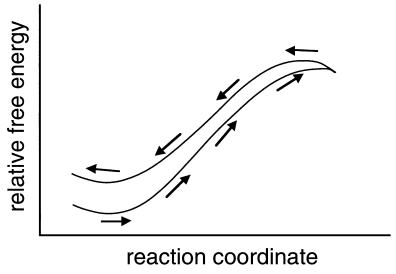

Fig. 6. Schematic representation of the hysteresis in a slow growth free energy plot. The arrows designate the direction of the scan in terms of the reaction coordinate.

incrementally changed from that in the previous time step. Formally speaking the system is never properly equilibrated unless the change in the RC is infinitesimally small (reversible change). However, the smaller the rate of change the better the approximation. Since the RC is changed at each time step, the force on the reaction coordinate is biased depending on the direction in which the RC is varied. Therefore a forward and reverse scan of the RC is likely to give different results as depicted in Fig. 6. This hysteresis, as it is called, is a direct consequence of the improper equilibration. Thus it is generally a good idea to perform both forward and reverse scans to reduce this error and to determine whether the rate of change of the reaction coordinate is appropriate. In other words, a slow growth simulation with virtually no hysteresis has its RC changed adequately slow, whereas a simulation with large hysteresis has its RC sampled too quickly. The advantage of the slow growth simulation is that the dynamics is not disrupted when the reaction coordinate is changed and hence the system only has to be thermally equilibrated once. On the other hand, the method has the disadvantage that both the forward and reverse scans should be performed.

It should be noted that although the forces at each time step are determined from a full quantum mechanical electronic structure calculation, the dynamics itself is still classical. Therefore, quantum dynamical effects such as the tunneling are not included in the estimates of the reaction free energy barriers. Since the classical vibrational energy levels are continuous, $H_{vib}=\sum RT/2$ for all states, the zero point energy correction and ΔH_{vib} are also not included in the free energy barriers derived from the AIMD simulation.

4.5. Issues with configurational sampling

In order to properly sample the canonical ensemble, the system must be thermally equilibrated. Thermal equilibration often done by equilibrating the system at a particular temperature for a few picoseconds thereby ensuring that all vibrational modes are excited to an equal extent. Since we cannot afford to let the system thermally equilibrate for such a long period before we begin sampling, we take an alternative approach. To efficiently achieve a thermally equilibrated system, the nuclei are excited by a series of sinusoidal pulses. Each of the excitation vectors is chosen to be orthogonal to the already excited modes, thereby ensuring an evenly distributed thermal excitation [40,41]. Another requirement in order to properly generate a canonical ensemble is that the temperature be held constant. The most common procedure and the procedure we use is to couple the system to a heatbath by the Nosé thermostat method [42]. Applying a separate thermostat to both the wavefunction coefficients and the nuclei ensures a proper NVT ensemble is sampled.

Since the configurational averages in classical molecular dynamics do no depend on the masses of the nuclei [43], a common technique to increase the sampling rate involves replacing the true masses with more convenient ones. Since nuclear velocities scale with $m^{-1/2}$, smaller masses move faster and therefore potentially sample configuration space faster. As a result, the masses of the heavy atoms can be scaled down in order to increase sampling. For example, we commonly rescale the masses of C, N and O in our simulations from 12, 14 and 16 amu, respectively, to 2 amu. There is a limit to the mass reduction, because at some point the nuclei move so fast that the time step has to be reduced. At this point there is no gain in reducing the masses further because if the time step has to be shortened, we have to perform more time steps to achieve the same amount of sampling. It is for this reason, we generally scale our hydrogen masses up from 1 to 1.5 amu or higher in order to use a larger time step.

5. Ab initio molecular dynamics as a practical tool for studying catalysis

Margl and coworkers [44–48] have investigated several transition metal-based homogenous catalytic

systems with PAW AIMD. Recently, we have applied PAW to examine the chemistry of a Ti(IV) metallocene olefin polymerization catalyst. In studying this system we have found that ab initio molecular dynamics can be used to

1. determine the timescales of processes,
2. efficiently explore complicated free energy surfaces in a synergistic fashion with traditional static methods,
3. find new reactions, and
4. to provide a general way of determining finite temperature free energy barriers.

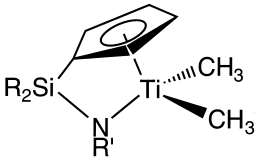

1

Metallocene catalyzed olefin polymerization technology is expected to revolutionize the immense polyolefin industry. Amongst the first metallocene catalysts to have been commercialized [49] are the mono Cp "constrained-geometry" catalysts of the form $(CpSiR'_2NR)Ti–X_2$, where $X=CH_3$, Cl (e.g. 1). For most group 4 metallocenes, the catalytic resting state is believed to be a cationic metal alkyl complex, e.g. $(CpSiR'_2NR')Ti–R^+$, where R represents the growing alkyl chain. Commencing from the resting state Ti-alkyl complex, Fig. 7 depicts the assumed and well-established Cossée–Arlman mechanism for the chain growth. Addition of olefin to the resting state forms an olefin π-complex. From the π-complex a four centered transition state is formed whereby the olefin inserts into the $Ti–C_\alpha$ bond. The initial or kinetic product is a γ-agostic Ti–alkyl complex. In "static" studies [50] of similar bis-Cp zirconocene catalysts, the initial γ-agostic complex is believed to rapidly rearrange to the more favorable β-agostic resting state complex. Olefin uptake and insertion therefore likely commences from the β-agostic complex as opposed to the γ-agostic complex. Therefore, to study the insertion process, it is important to know the structure of the resting state.

5.1. *Studying fluxionality and timescales with AIMD*

With the intent of studying the nature and fluxionality of the resting state we have performed an AIMD simulation where R was modeled by a propyl chain [48]. A propyl group was used as a model for the growing chain in order to investigate the possible rearrangement of the assumed γ-agostic kinetic product of the insertion. Initiated from a γ-agostic Ti–propyl complex, a 4 ps simulation at 300 K was performed. In order to enhance the sampling, the masses were rescaled to 5.0 (Ti), 2.0 (Si, N and C), and 1.5 (H) atomic mass units. Therefore, the timescales are fictitious and the 4 ps simulation is approximately equivalent to a 7 ps simulation.

The MD simulation revealed that there was rapid interconversion between β- and γ-agostic Ti–alkyl complexes. The right-hand side of Fig. 8 shows two snapshot structures from the simulation representative of the γ-agostic complex and the β-agostic complex. The two graphs in Fig. 8 trace structural quantities during the dynamics important in characterizing the resting state. Graph (a) follows the $Ti–H_\gamma$ distance while (b) follows the $Ti–H_\beta$ distances, with the shaded regions indicating the formation of γ- and β-agostic bonds, respectively. The trajectory reveals that the propyl chain rapidly interconverts between the γ- and β-agostic alkyl complexes, spending roughly equal time in each of the conformations. Although

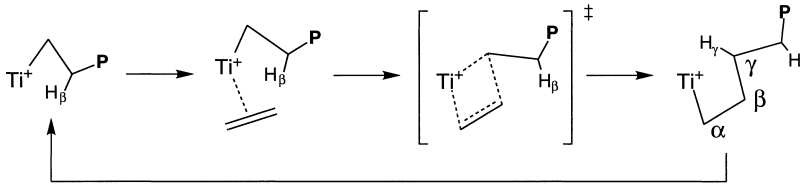

Fig. 7. Cossée–Arlman [51,52] mechanism for chain propagation in Ziegler–Natta and single-site olefin polymerization catalysts.

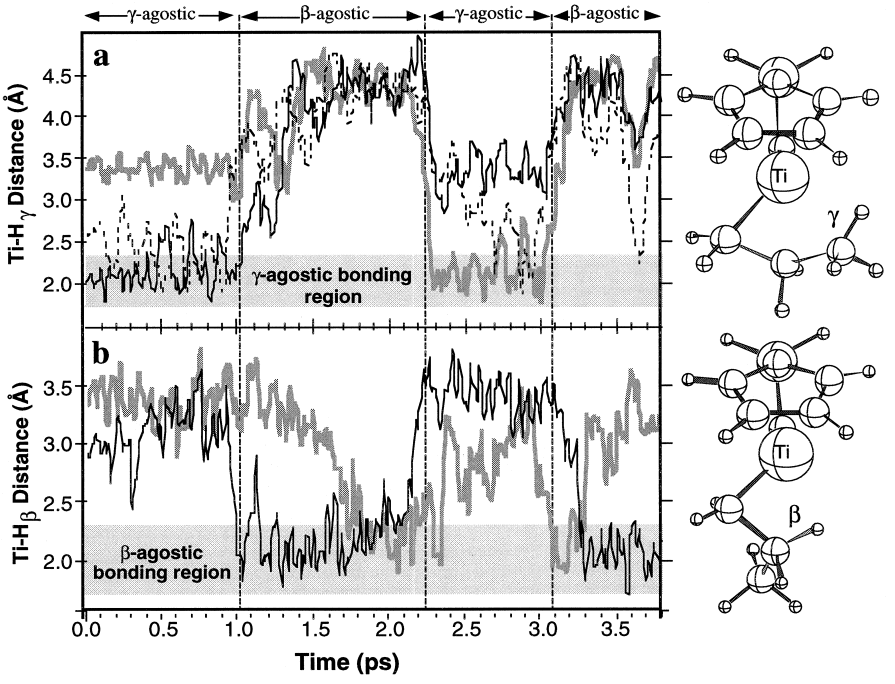

Fig. 8. Selected structural quantities as a function of the simulation time for the AIMD simulation of the Ti-propyl model of the resting state. Shaded regions in graphs (a) and (b) indicate agostic bonding. Vertical lines separate where the Ti-propyl cation can be characterized as γ- and β-agostic complexes. Shown to the right of the graphs are two snap shot structures from the simulation characteristic of the γ- and β-agostic complexes.

the timescales in the AIMD simulation are fictitious because of the mass rescaling, the simulation does demonstrate that the fluctuation of the resting state alkyl complex is extremely rapid. The graphs in Fig. 8 also show that there is always an agostic interaction present. When the_γ-agostic bond is lost, it is immediately replaced by another γ-agostic bond or a β-agostic bond. Thus, the strong preference for the formation of agostic interactions demonstrates the stabilization accrued from these interactions. Another excellent demonstration of the PAW AIMD method to study fluxionality and timescales is that of Margl and coworkers [53] who have examined the dynamics of beryllocene.

5.2. *Using AIMD to chart reaction paths on flat potential surfaces*

We have used AIMD to chart reaction pathways in systems with high configurational variability. Such ''flat'' potential energy surfaces are often difficult and tedious to explore with conventional static methods. By using the slow growth technique, AIMD can be utilized to initially scan the optimal reaction pathway. As demonstrated by the simulation of the resting state in Fig. 8, the potential energy surface associated with the constrained geometry system exhibits these problematic traits. In studying the olefin insertion process in the constrained geometry catalyst, initial static calculations revealed that there were at least four β-agostic π-complexes that were all within a small 10 kJ/mol range. Rather than explore the insertion process commencing from each of the four π-complexes, the insertion process was mapped out using the slow growth method whereby an ethene molecule was gradually inserted into the Ti–C bond of the Ti-propyl^{+} resting state. In this simulation the distance between the C_α and the midpoint of the C–C bond of the ethene was used as the slow growth reaction coordinate. A rapid 20 000 time step simulation was performed where the RC was varied from 5.1 Å, a distance in which the incoming olefin is too far to form

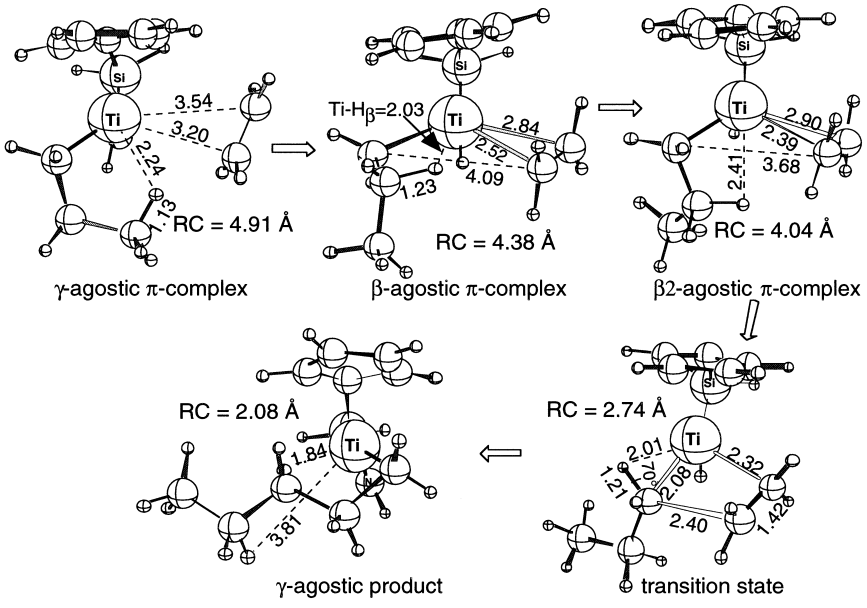

Fig. 9. Selected snapshot structures from the AIMD slow growth simulation of the olefin insertion in the constrained geometry catalyst. The snapshots provide qualitative picture of the insertion mechanism. The reaction coordinate (RC) used in the simulation was the distance between the α carbon of the Ti-alkyl moiety and one of the carbon atoms of the olefin.

a strong π-bond, to a value of 1.9 Å. Again the simulation was thermostated at 300 K and the masses were rescaled as in the previous resting state simulation.

Fig. 9 depicts several snapshots of the simulation which provides a qualitative picture of the insertion process. More detailed monitoring of the structural and energetic quantities can be found in [48] and are not shown here. Since the simulation was initiated from the γ-agostic alkyl complex, a weak γ-agostic π-olefin complex is formed in the early stages of the simulation. The first snap shot structure in Fig. 9 taken at a reaction coordinate value of 4.91 Å is indicative of the early complexation. As the olefin is drawn closer, the γ-agostic π-complex gives way to an ''in-plane'' β-agostic π-complex where the olefin carbon atoms and the β-hydrogen are coplanar. The second snapshot structure at RC=4.38 Å is representative of this ''in-plane'' β-agostic complex. As the RC is further contracted, β-methylene group rotates out of the coordination plane in order to allow for the α-carbon and the olefin carbon bond to form. Such a ''out-of-plane'' β-agostic π-complex is shown in Fig. 9 with a RC=4.04 Å. From here, the transition state and the γ-agostic product are formed at approximately RC=2.74 Å and RC=2.08 Å, respectively.

Using the AIMD simulation as a guideline, stationary points along the potential surface were mapped with traditional static methods. (Eventually, the insertion process commencing from all four initial β-agostic π-complexes was examined.) The lowest energy insertion pathway was indeed found to follow essentially the same pathway as resolved from the MD simulation. Stationary points corresponding to each of the structures in Fig. 9 along the insertion pathway were located which provided an accurate energetic picture of the potential surface. This application demonstrates that the AIMD method can be utilized effectively in a cooperative fashion with the traditional static methods.

5.3. New reaction pathways with AIMD

In studying the β-hydride elimination process in the constrained-geometry catalyst with a slow growth simulation, the PAW AIMD simulation generated an unexpected but more energetically favorable reaction which the static calculations did not detect. The product turned out to be the most favorable unimolecular chain termination process which was later observed experimentally. Fig. 10 shows the β-hydride

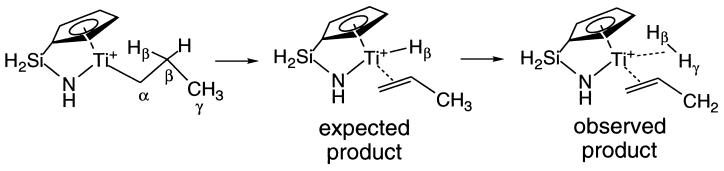

Fig. 10. Chain termination initiated from the β-agostic alkyl complex was expected to give rise to a olefin–hydride complex. Instead, as shown by the molecular dynamics simulation, the olefin–hydride complex was only briefly formed before giving rise to a more stable alkyl dihydrogen complex.

elimination process that was to be examined and the allyl dihydrogen formation process that was actually observed.

A slow growth simulation designed to determine the reaction free energy at 300 K of the β-hydride elimination process to form a olefin–hydride complex was performed [54,55]. In this simulation the distance from C_β to the H_β–H_β midpoint was used as the reaction coordinate. Commencing from the β-agostic alkyl complex the C_β–H_β distance expanded during the simulation. Plotted in Fig. 11 are various structural and electronic quantities which best characterizes the reaction observed. Up to a reaction coordinate value of approximately 1.6 Å, the expected β-elimination process progresses as anticipated. However, at a reaction coordinate value of roughly 1.6 Å all of the quantities traced in Fig. 11 change dramatically, marking the rapid formation of the allyl–dihydrogen complex from the transient olefin hydride complex. Graph (a) shows the rapid formation of the dihydrogen bond with the simultaneous breaking of the C_γ–H_γ bond. The Ti–C distances in graph (b) illustrates the change in the bonding description between the C_3 fragment and the Ti center. With two short and one long Ti–C distances a β-agostic alkyl interaction dominates the initial part of the simulation. When the allyl complex forms, all three Ti–C bond distances converge suggesting the η^3 bonding pattern of the allyl. Plot (c) follows the net ESP fitted charges on the Ti, H_β and H_γ atoms, again revealing an abrupt change at approximately RC=1.6 Å. The sudden deionization of the Ti center suggests that the formation of the allyl moiety stabilizes the complex through electron donation to the Ti center.

Static calculations on the olefin–hydride and the allyl–dihydrogen complex reveal that the allyl–dihydrogen complex is in fact 22 kJ/mol more stable than the olefin–hydride suggesting that the unimolecular β-

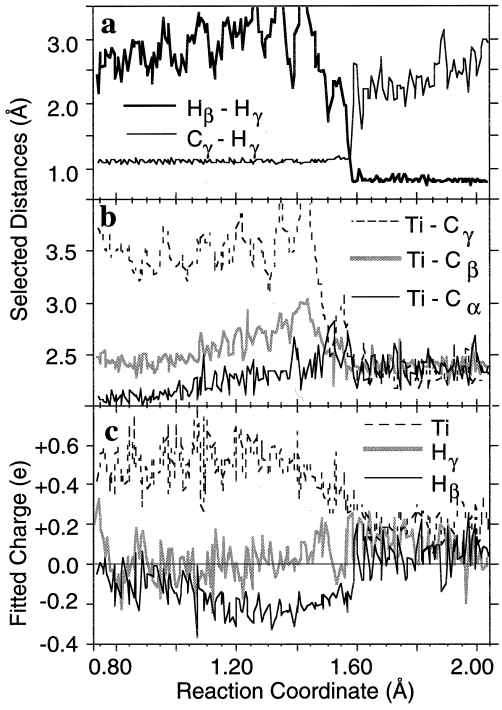

Fig. 11. Selected structural and electronic quantities as a function of the reaction coordinate for the slow growth simulation of the uni-molecular chain termination process. The dramatic change in the plotted quantities at a RC value of 1.6 Å marks the formation of the unexpected allyl–dihydrogen complex.

elimination process does not form an olefin hydride, but in fact produces dihydrogen and an Ti–allyl complex. Spurious formation of hydrogen gas has been observed in slurry phase metallocene catalyzed olefin polymerization experiments [56,57] providing experimental evidence of the allyl formation.

It is important to state that the actual thermodynamic product of β-hydrogen elimination – namely the allyl dihydrogen complex – was first located by AIMD simulations and would not have been found

otherwise by us. This shows the uniquely powerful predictive ability of the AIMD method, which searches configuration space more globally instead of locally and thus has a greater chance of hitting unexpected, but important, reaction paths and products.

5.4. *Reaction free energy barriers with the slow growth AIMD simulations*

The previous examples nicely demonstrate that the slow growth technique can be used to chart "difficult" potential energy surfaces for static calculations. As previously outlined in Section 4.4, the slow growth method can also be used to estimate free energy barriers by means of thermodynamic integration. We have applied the slow growth technique to estimate the free energy barriers at 300 K of four chain termination processes associated with the constrained geometry catalyst. Illustrated in Fig. 12 are the four processes: (a) hydrogen transfer to the monomer, (b) β-hydrogen elimination, (c) olefinic C–H activation and (d) is an alkyl C–H activation. Since this method for the determination of reaction free energy barriers is somewhat novel, free energy barriers of the same four processes were then calculated using more established "static" methods and compared.

For processes (a), (c) and (d) which involve the transfer of a hydrogen from one carbon to another a special mid-plane reaction coordinate was developed. The "mid-plane" reaction coordinate is depicted in Fig. 13. If C_1 is the carbon the hydrogen atom is initially bound to and C_2 is the carbon atom that the hydrogen is to be transferred to, then the mid-plane plane reaction coordinate is defined as the ratio r/R, where R is the length of the vector between C_1 and C_2 and r is the length of the projection of the C_1–H vector onto the vector **R**. The reaction coordinate constrains the H atom to lie on the plane perpendicular to and passing through the end point of the vector **r**. When the mid-plane RC is small, the hydrogen is still bound to C_1 while when it is equal to 0.5 the hydrogen

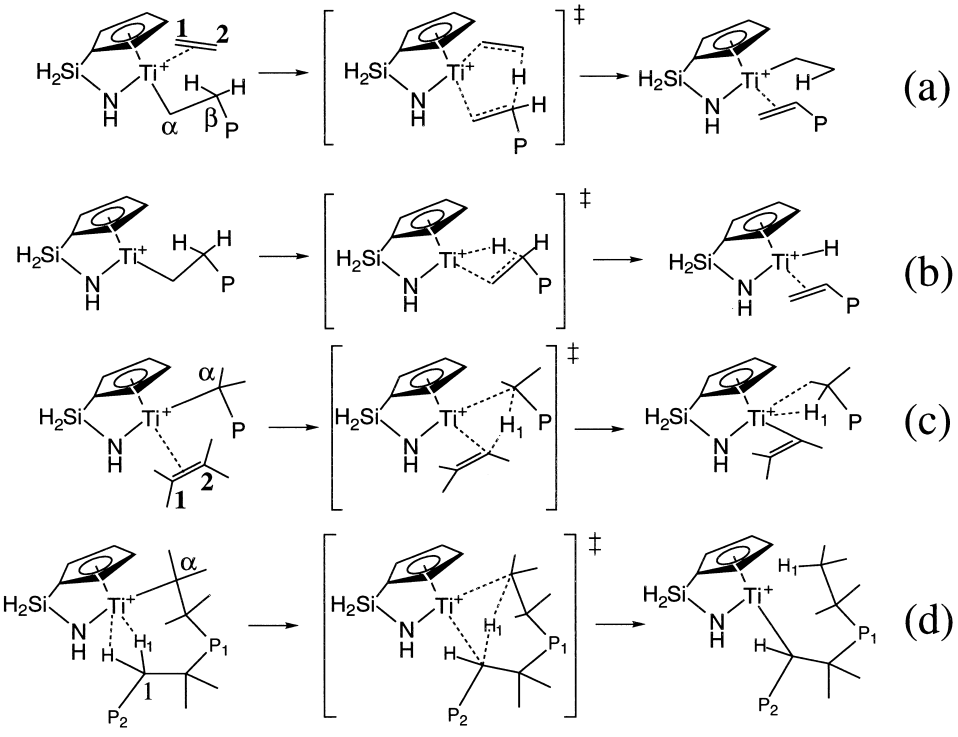

Fig. 12. Four chain termination processes studied with the slow growth AIMD method in order to estimate reaction free energy barriers. (a) Hydrogen transfer to the monomer, (b) β-hydrogen elimination, (c) olefinic C–H activation and (d) is a alkyl C–H activation.

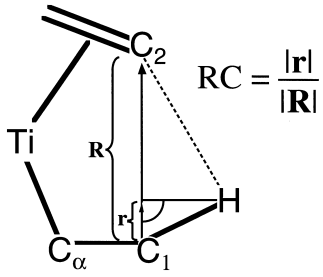

Fig. 13. Definition of the mid-plane reaction coordinate.

lies halfway between the two carbons. The mid-plane constraint was used because it is presumed to be the most reversible reaction coordinate for the transfer process and therefore the least susceptible to large hysteresis. For process (b) the hydrogen transfer to the metal, the distance from C_β to the center of mass of the two H_β atoms was utilized as the slow growth reaction coordinate.

In each of the simulations the system was thermostated at 300 K and the masses were rescaled as in previous simulations of the Ti constrained-geometry catalyst. About 35 000 time steps were performed for each simulation or approximately 6 ps of real time (9–12 ps when mass rescaling is considered). Both forward and reverse scans were performed from the reactant to the approximate transition state. In the static calculations, reactants and transition states were fully optimized without constraints. Frequency calculations were performed on each of the stationary points and the calculation of the free energies followed standard text book procedures [58]. Full details of the calculations can be found in [47].

Table 2 compares the free energy barriers of the static calculations to those obtained by the Car–Parrinello simulations. It is important to note that although the Car–Parrinello method involves a quantum mechanical calculation to determine the electronic structure, the actual dynamics is purely classical in nature. Therefore, quantum dynamical effects such as the zero-point energy correction are not accounted for. As a result, in Table 2 there are two columns referring to the static calculations, one with all of the quantum dynamical effects eliminated for a more proper comparison and one with the quantum effects included. Although there are several important differences in the two simulations, the static and dynamic free energy barriers are in remarkable agreement with one another. The mean absolute deviation between dynamically and ''statically'' (i.e. from the partition function of a harmonic oscillator) derived $\Delta F^{\ddagger}$ values is 3.3 kJ/mol (signed mean: −0.3 kJ/mol), and 8.8 kJ/mol (signed mean: −6.6 kJ/mol) if one corrects for the terms not present in the molecular dynamics simulations.

These results clearly demonstrate that the molecular dynamics simulations both complement and further corroborate the results of the static calculations well.

Table 2
Comparison of the ''static'' and ''dynamic'' reaction free energy barriers

Process	Free energy barrier $\Delta F^{\ddagger}$ (kJ/mol) at 300 K		
	Car–Parrinello simulation[a,b]	Static[c]	Static with quantum effects[d]
(a) Hydrogen transfer to monomer[e]	43±8	43.0	40.1
(b) Hydrogen transfer to metal[f]	57±3	65.4	53.9
(c) Olefin σ-bond metathesis[e]	87±5	93.8	91.7
(d) Alkyl σ-bond metathesis[e]	70±3	81.2	72.3

[a] Does not include any quantum dynamical corrections such as zero-point energy correction. Additionally, since the classical vibrational energy levels are continuous, $H_{vib}=\sum RT/2$ and $\Delta H_{vib}=0$ for the MD simulations.

[b] Reported values are the average of the forward and reverse scans. The reported error bars are half the difference between the forward and reverse scans.

[c] Does not include zero-point energy correction and ΔH_{vib} to more correctly compare with Car–Parrinello MD free energies ($\Delta F=\Delta H_{el}-T\Delta S_{total}$).

[d] Includes zero-point energy correction and ΔH_{vib} ($\Delta F=\Delta H_{el}+\Delta H_{vib}+\Delta ZPE-T\Delta S_{total}$). Does not include quantum tunneling.

[e] An ethyl group is used to model growing chain in the static simulation whereas a propyl group is used to model the growing chain in the molecular dynamics simulation.

[f] A propyl group is used to model the growing chain in both static and dynamic simulations.

The Car–Parrinello molecular dynamics method provides a general method of calculating accurate free energy barriers that are in excellent agreement with established static methods. We reiterate here that the Car–Parrinello simulations do not include any quantum dynamical effects. However, it is apparent from Table 1 that the *relative* vibrational enthalpies and zero-point energies are a minor factor in the reactions studied. Finally, we point out that both static and dynamic methods do not account for quantum tunneling effects.

Plotted in Fig. 14(a) is the free energy profile obtained from the forward and reverse slow growth simulation of the alkyl σ-bond metathesis chain termination reaction displayed in Fig. 12(d). For this process the hysteresis is small with the forward and reverse estimates of the reaction free energy barrier differing by only 6 kJ/mol. Furthermore, in both cases the transition state occurs at the reaction coordinate value of RC=0.5. The average slow growth value of 70 kJ/mol is in reasonable agreement with the static free energy barrier of 81 kJ/mol when all quantum effects, not taken into account in the AIMD simulation are factored out. When the quantum effects in the static estimate are included the free energy barrier of 72 kJ/mol is in better agreement with the slow growth result.

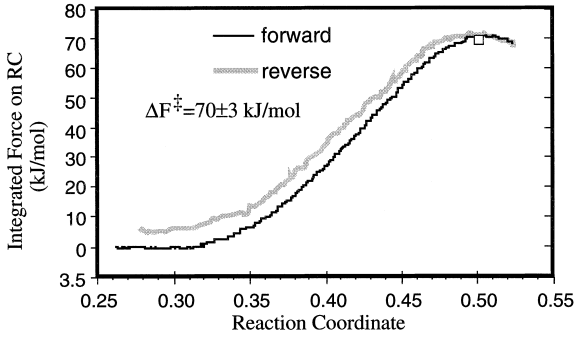

Fig. 14. The integrated force on the reaction coordinate traced as a function of the mid-plane reaction coordinate for the AIMD simulation the alkyl σ-bond metathesis chain termination reaction. The box on the forward scan marks the point in the simulation at which the snap shot structure shown in Fig. 15 is taken from.

Shown in Fig. 15 is the optimized transition state structure from the static calculation and a snapshot structure taken from the transition state region of the forward scan of the slow growth simulation. The similarity in the two structures is striking, further showing that the AIMD slow growth method for determining reaction barriers provides results in good agreement with more established static techniques.

6. Combined QM/MM ab initio molecular dynamics

The combined QM/MM methodology can be easily embedded within the Car–Parrinello framework allowing for ab initio molecular dynamics simulations of extended systems to be performed efficiently. We have implemented the combined QM/MM methodology of Singh and Kollman [1] within the PAW code by

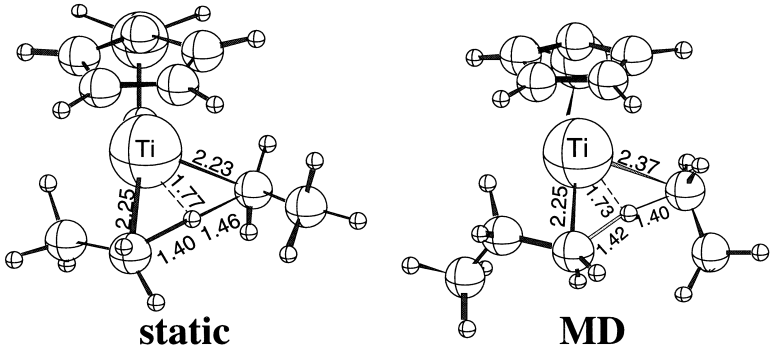

Fig. 15. Comparison of the static and dynamic transition state structures for the alkyl σ-bond metathesis chain termination reaction. The static structure is a fully optimized transition state whereas the MD structure is simply a snap shot structure extracted from the forward scan of the slow growth simulation.

extending the Car–Parrinello Lagrangian (Eq. (6)) to include the MM subsystem:

$$\mathscr{L} = \sum \mu_i \langle \dot{\Psi}_i | \dot{\Psi}_i \rangle + \tfrac{1}{2} \sum M_{I,\mathrm{QM}} \dot{R}^2_{I,\mathrm{QM}} - E_{\mathrm{DFT}}(|\Psi\rangle, R_{\mathrm{QM}}) + \sum_{i,j} \Lambda_{ij} \big(\langle \Psi_i | \Psi_j \rangle - \delta_{ij} \big) + \tfrac{1}{2} \sum M_{I,\mathrm{MM}} \dot{R}^2_{I,\mathrm{MM}} - E_{\mathrm{MM}}(R_{\mathrm{QM}}, R_{\mathrm{MM}}). \quad (12)$$

The last two terms in Eq. (12) are the kinetic energy of the MM nuclei and the potential energy derived from the MM force field. With the intent of validating the combined ab initio molecular dynamics Car–Parrinello QM/MM methodology we have applied the method to determine the free energy barrier of the hydrogen transfer to the monomer chain termination process (Fig. 4). As in the static QM/MM calculations presented in Section 3, the bulky R=Me and Ar=2,6-$C_6H_3(i\text{-Pr})_2$ groups were treated by a molecular mechanics potential whereas the Ni-diimine core including the growing chain and monomer will be treated by a density functional potential. Full details of the simulation can be found in [59].

Plotted in Fig. 16(a) is the free energy profile for the QM/MM AIMD simulation and the pure QM simulation without the bulky ligands. As expected there is a dramatic increase in the termination barrier when the bulky ligands are added. The estimated free energy barrier of 62 kJ/mol at 300 K is in good agreement with the experimental value [19] of ∼67 kJ/mol at 272 K. Plotted in Fig. 16(b) are various structural quantities that characterize the transfer process. Plotted in graph (c) is the relative molecular mechanics van der Waals energy for the interactions between the bulky aryl ligands and the active site propyl and ethene group. This plot reveals that the steric interaction between the active site moieties and the aryl ligands increases as the hydrogen transfer process occurs. This is a result of the expansion of the active site during the hydrogen transfer process. Displayed in Fig. 17 is a snapshot structure of the slow growth simulation taken from the transition state region. The analogous transition state structure from a static QM/MM calculation is shown in Fig. 5(a). Again there is a strong similarity in the static and dynamic results.

The applicability of the combined QM/MM ab initio molecular dynamics approach to study large transition metal catalytic systems has been demonstrated. In applications where static QM/MM methods may be inadequate the QM/MM MD methodology shows particular promise. One such application is to reactions which have no enthalpic barrier on the static 0 K potential surface. The capture of the monomer in the Brookhart catalyst system as shown in Fig. 4 is one such case [30,31]. Another promising area of application, which we intend to explore in the future, is the simulation of solvent effects in chemical reactions. With the inclusion of electrostatic coupling into this method such that the electronic structure of the QM system (solute) can be polarized by electrostatic influences in the MM system (solvent), the influence

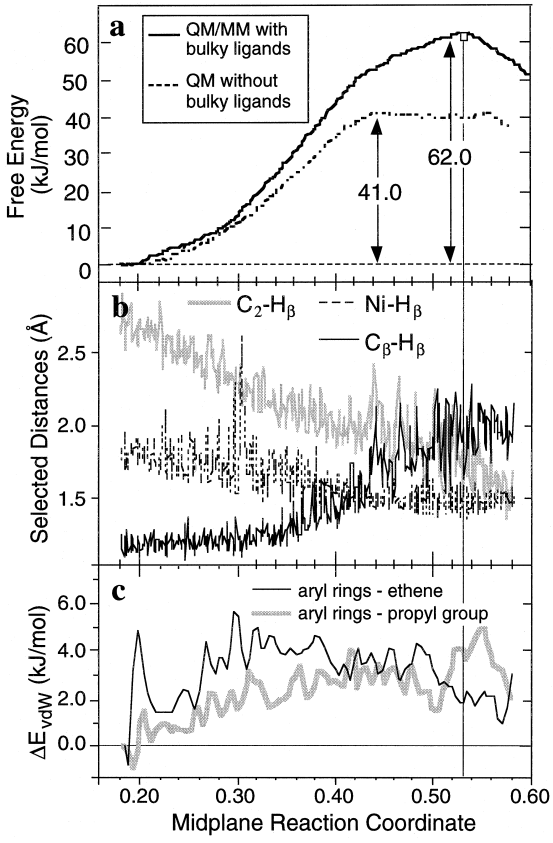

Fig. 16. Selected structural and energetic quantities as a function of the reaction coordinate from the combined QM/MM simulation. (a) and (b) Selected distances. (c) The molecular mechanics van der Waals interaction energies between the two bulky aryl groups and the active site ethene and propyl groups relative to the resting state value. The energies plotted have been "smoothed" and are the running average over 500 time steps.

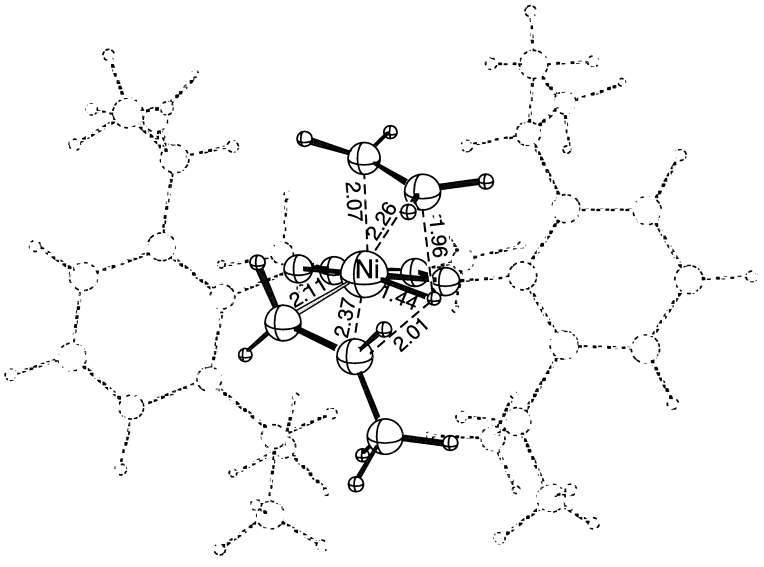

Fig. 17. Snapshot structure extracted from the transition state region of the QM/MM AIMD simulation of the chain termination process in the Brookhart Ni-diimine catalyst. The snapshot structure is denoted by a vertical line in Fig. 16. Conventions as in Fig. 5.

of solvent can be approximated. Such coupling is currently being developed and validated in our lab.

7. Concluding remarks

With the methodologies presented here, the combined QM/MM method and the ab initio molecular dynamics method, we are moving towards more realistic computational simulations of complex systems. The QM/MM method allows for the simulation of large systems at the ab initio level without completely neglecting the groups and substituents not within the active site. As demonstrated by our QM/MM calculations of the Brookhart polymerization catalyst, these outer groups can often play a crucial role in the chemistry. Since the stereoselectivity in many heterogeneous and homogenous catalytic systems is controlled by steric interactions there is great potential for the combined QM/MM method to be utilized effectively in such areas. The ab initio molecular dynamics method also shows great potential for becoming a standard computational chemistry tool particularly for exploring processes which have a high degree of configurational variability. We have applied the methodology to several transition metal-based homogenous catalytic systems, clearly demonstrating the usefulness of the method. The union of the two methods, the combined QM/MM ab initio molecular dynamics method, allows finite temperature simulations to be performed on extended aperiodic systems. With electrostatic coupling, the combed QM/MM molecular dynamics method is a very promising tool for including solvent effects. Indeed with the combination of these techniques we are developing more realistic models of catalytic systems which can take into account large ligands, finite temperature effects and potentially solvent effects. Although we have demonstrated all the methodologies on homogenous catalytic systems, all of the methods are quite amicable to being applied to heterogeneous systems.

Acknowledgements

It is a pleasure to thank Peter Blöchl of IBM Zurich for his numerous contributions. This work has been supported by the National Sciences and Engineering Research Council (NSERC) of Canada, as well as by the donors of the Petroleum Research Fund, administered by the American Chemical Society (ACS-PRF No. 31205-AC3) and by Novacor Research and Technology Corporation (NRTC) of Calgary. TKW wishes to thank NSERC, the Alberta Heritage Scholarship

Fund and the Izaak Walton Killam memorial foundation for financial support.

References

[1] U.C. Singh, P.A. Kollman, J. Comp. Chem. 7 (1986) 718.
[2] M.J. Field, P.A. Bash, M. Karplus, J. Comp. Chem. 11 (1990) 700.
[3] F. Maseras, K. Morokuma, J. Comp. Chem. 16 (1995) 1170.
[4] J. Gao, in: K.B. Lipkowitz, D.B. Boyd (Eds.), Reviews in Computational Chemistry, vol. 7, VCH, New York, 1996.
[5] D. Bakowies, W. Thiel, J. Phys. Chem. 100 (1996) 10580.
[6] J. Gao, X. Xia, Science 258 (1992) 631.
[7] J. Gao, J. Phys. Chem. 96 (1992) 537.
[8] A. Warshel, M. Levitt, J. Mol. Biol. 103 (1976) 227.
[9] V. Théry, D. Rinaldi, J.-L. Rivail, B. Maigret, G.G. Ferenczy, J. Comp. Chem. 15 (1994) 269.
[10] D. Bakowies, W. Thiel, J. Comp. Chem. 17 (1996) 87.
[11] L.L. Ho, A.D. MacKerell Jr., P.A. Bash, J. Phys. Chem. 100 (1996) 4466.
[12] D.S. Hartsough, K.M. Merz Jr., , J. Phys. Chem. 99 (1995) 11266.
[13] P.D. Lyne, A.J. Mulholland, W.G. Richards, J. Am. Chem. Soc. 117 (1995) 11345.
[14] M.J. Harrison, N.A. Burton, I.H. Hillier, I.R. Gould, Chem. Commun. (1996) 2769.
[15] P.A. Bash et al., Biochemistry 30 (1991) 5826.
[16] T. Matsubara, F. Maseras, N. Koga, K. Morokuma, J. Phys. Chem. 100 (1996) 2573.
[17] L. Deng, T.K. Woo, L. Cavallo, P.M. Margl, T. Ziegler, J. Am. Chem. Soc. 119 (1997) 6177.
[18] J. Haggin, Chem. Eng. News 5 (1996) 6.
[19] L.K. Johnson, C.M. Killian, M. Brookhart, J. Am. Chem. Soc. 117 (1995) 6414.
[20] L.K. Johnson, S. Mecking, M. Brookhart, J. Am. Chem. Soc. 118 (1996) 267.
[21] W.D. Cornell, P. Cieplak, C.I. Bayly, I.R. Gould, D.M. Ferguson, D.C. Spellmeyer, T. Fox, J.W. Caldwell, P.A. Kollman, J. Am. Chem. Soc. 117 (1995) 5179.
[22] E.J. Baerends, D.E. Ellis, P. Ros, Chem. Phys. 2 (1973) 41.
[23] E.J. Baerends, P. Ros, Chem. Phys. 2 (1973) 52.
[24] A. Becke, Phys. Rev. A 38 (1988) 3098.
[25] J.P. Perdew, Phys. Rev. B 34 (1986) 7406.
[26] J.P. Perdew, Phys. Rev. B 33 (1986) 8822.
[27] L. Deng, P.M. Margl, T. Ziegler, J. Am. Chem. Soc. 119 (1997) 1094.
[28] Professor M. Brookhart, Department of Chemistry, University of North Carolina at Chapel Hill, private communication.
[29] W. Keim, Angew. Chem., Int. Ed. Engl. 29 (1990) 235.
[30] L. Deng, T. Ziegler, T.K. Woo, P.M. Margyl, L. Fan, Organometallics 17 (1998) 3240–3253.
[31] T.K. Woo, Ph.D. Thesis, Department of Chemistry, University of Calgary, 1998.
[32] R. Car, M. Parrinello, Phys. Rev. Lett. 55 (1985) 2471.
[33] P.E. Blöchl, P.M. Margl, K. Schwarz (Eds.), ACS Symposium Series 629: Chemical Applications of Density-Functional Theory, vol. 629, American Chemical Society, Washington, DC, 1996.
[34] P.E. Blöchl, J. Chem. Phys. 103 (1995) 7422.
[35] P.E. Blöchl, Phys. Rev. B 50 (1994) 17953.
[36] D.L. Beveridge, F.M. DiCapua, Ann. Rev. Biophys. Chem. 18 (1989) 431.
[37] E.A. Carter, G. Ciccotti, J.T. Hynes, R. Kapral, Chem. Phys. Lett. 156 (1989) 472.
[38] E. Paci, G. Ciccotti, M. Ferrario, R. Kapral, Chem. Phys. Lett. 176 (1991) 581.
[39] T.P. Straatsma, H.J.C. Berendsen, J.P.M. Postma, J. Chem. Phys. 85 (1986) 6720.
[40] P. Margl, unpublished work.
[41] P.E. Blöchl, PAW User's Manual, IBM Research Division, Zurich Research Laboratory, Säumerstr. 4, CH-8803 Rüschlikon, Switzerland, 1998.
[42] S. Nosé, Mol. Phys. 52 (1984) 255.
[43] B. De-Raedt, M. Sprik, M.L. Klein, J. Chem. Phys. 80 (1984) 5719.
[44] P. Margl, P. Blöchl, T. Ziegler, J. Am. Chem. Soc. 117 (1995) 12625.
[45] P. Margl, P. Blöchl, T. Ziegler, J. Am. Chem. Soc. 118 (1996) 5412.
[46] P. Margl, J.C.W. Lohrenz, P. Blöchl, T. Ziegler, J. Am. Chem. Soc. 118 (1996) 4434.
[47] T.K. Woo, P.M. Margl, P.E. Blöchl, T. Ziegler, Organometallics 16 (1997) 3454.
[48] T.K. Woo, P.M. Margl, J.C.W. Lohrenz, P.E. Blöchl, T. Ziegler, J. Am. Chem. Soc. 118 (1996) 13021.
[49] K.F. Lindsay, in: Modern Plastics, 1993, p. 82.
[50] J.C.W. Lohrenz, T.K. Woo, T. Ziegler, J. Am. Chem. Soc. 117 (1995) 12793.
[51] P. Cossée, J. Catal. 3 (1964) 80.
[52] E.J. Arlman, P. Cossee, J. Catal. 3 (1964) 99.
[53] P.M. Margl, K. Schwarz, P.E. Blöchl, J. Chem. Phys. 103 (1995) 683.
[54] P.M. Margyl, T.K. Woo, P.E. Blöchl, T. Ziegler, J. Am. Chem. Soc. 120 (1998) 2174–2175.
[55] T.K. Woo, Ph.D. Thesis, Department of Chemistry, University of Calgary, 1998.
[56] F.J. Karol, S.-C. Kao, E.P. Wasserman, R.C. Brady, Z. Yu, New J. Chem., accepted.
[57] E.P. Wasserman, Union Carbide Corporation, Polymers Research and Development, PO Box 670, Bound Brook, NJ 08805, USA, private communication.
[58] D.A. McQuarrie, Statistical Thermodynamics Harper and Row, New York, 1973.
[59] T.K. Woo, P.M. Margl, P.E. Blöchl, T. Ziegler, J. Phys. Chem. 101 (1997) 7877.
[60] A. Curioni, M. Sprik, W. Andreoni, H. Schiffer, J. Hutter, M. Parrinello, J. Am. Chem. 119 (1997) 7218.